Supplemental Data

for

Free Energy Landscape Remodeling for the Cardiac Pacemaker Channel Explains the Molecular Basis of Familial Sinus Bradycardia

Stephen Boulton[1], Madoka Akimoto[2], Sam Akbarizadeh[2] and Giuseppe Melacini[1,2,*]

[1] Department of Biochemistry and Biomedical Sciences, McMaster University

[2] Department of Chemistry and Chemical Biology, McMaster University

* Corresponding author email – melacin@mcmaster.ca

Materials and Methods

Fast *vs.* Slow Exchange Regime Assignment for Residues with Weak HSQC Intensities

For residues with weak HSQC peak intensities it is possible that at sub-stoichiometric ratios of cAMP the minor holo peak for slow exchanging residues may pass undetected, resulting in a single observable peak similarly to fast exchanging residues. To eliminate these ambiguities the assignment of fast *vs.* slow exchange regimes was corroborated through HSQC spectra acquired at a higher ligand:protein concentration ratio in order to increase the free ligand concentration (*i.e.* $[cAMP]_{free}$) and, based on equation (1), k_{ex}. The resultant increase in the k_{ex} value affects residues in the slow and fast exchange regimes differently. Slowly exchanging residues experience a shift toward the intermediate regime, causing line-broadening and a decrease in signal intensity (Fig S8A,B). In contrast, when a residue is in the fast exchange regime, an increase in the k_{ex} rate would not decrease its intensity (Fig S8C,D).

It is also notable that the faster cAMP on-off exchange observed for the S672R mutant relative to the WT limits the applicability of Nz-exchange experiments, which could in principle provide quantitative measurements of the on/off rates for cAMP. Furthermore, if higher cAMP concentrations were utilized to increase the holo fraction, the k_{ex} value would increase as well bringing most residues in the S672R mutant in the intermediate/fast exchange regime, where the Nz-exchange experiment does not apply. Due to these limitations, we could not utilized Nz-spectroscopy for measuring the cAMP binding kinetics and we reverted to the HSQC analysis outlined in the main text.

Calculation of On/Off Rates Starting from the $k_{ex.}$ And K_d Values.

On and off rates of cAMP binding (k_{on} & k_{off}) were computed from the k_{ex} and the K_d values as follows. Since:

$$K_d = k_{off}/k_{on} \qquad (S1)$$

Equation (1) for k_{ex} is re-arranged as:

$$k_{on} = k_{ex} / ([cAMP]_{free} + K_d) \qquad (S2)$$

$$k_{off} = k_{ex} / (([cAMP]_{free} / K_d) + 1) \qquad (S3)$$

The k_{ex} value is estimated based on the identification of the intermediate exchange regime within the scale defined by the sorted apo-holo Hz differences, as shown in Fig 5D-F. The K_d value was measured through the STD amplification actors (Fig S2), while $[cAMP]_{free}$ is obtained based on the total protein and ligand concentrations as well as the K_d value.

Supplementary Tables

Table S1. Gaussian Fitting of S^2 Order Parameter Distributions [a]

		Apo		*Holo*	
	Parameters	*WT*	*S672R*	*WT*	*S672R*
Single Gaussian	A (Height)	30.9	23.0	35.5	28.2
	B (Position)	0.90	0.86	0.92	0.92
	C (Width)	0.07	0.10	0.07	0.07
Two Gaussians	A1 (Height)	31.1	15.7	35.5	29.1
	B1 (Position)	0.91	0.90	0.92	0.92
	C1 (Width)	0.07	0.05	0.07	0.07
	A2 (Height)	3.9	13.5	$< 10^{-8}$	4.7
	B2 (Position)	0.68	0.80	0.18	0.73
	C2 (Width)	0.04	0.12	0.09	0.03

[a] The functions subject to non-linear fitting were: $A*\exp(-(S^2-B)^2/2C^2)$ for a single Gaussian or $A1*\exp(-(S^2-B1)^2/2C1^2) + A2*\exp(-(S^2-B2)^2/2C2^2)$ for two Gaussians.

Table S2. Reduced Spectral Density Statistics for Apo WT and Apo S672R HCN4 (563-724) Samples

		$J(0) \times 10^9$ (s/rad)		$J(\omega_N) \times 10^{10}$ (s/rad)		$J(\omega_N + \omega_H) \times 10^{11}$ (s/rad)	
Region	**Residues**	**WT**	**S672R**	**WT**	**S672R**	**WT**	**S672R**
Total	563-724	3.82 ± 0.21	3.35 ± 0.45	1.69 ± 0.12	1.72 ± 0.11	0.56 ± 0.15	0.61 ± 0.13
β2-β3	621-636	4.32 ± 0.28	4.41 ± 0.94	1.56 ± 0.15	1.55 ± 0.19	0.23 ± 0.20	0.46 ± 0.23
BBR	639-652	3.79 ± 0.20	3.35 ± 0.48	1.62 ± 0.13	1.65 ± 0.12	0.43 ± 0.16	0.37 ± 0.13
PBC	659-676	3.85 ± 0.24	4.28 ± 0.75	1.65 ± 0.10	1.74 ± 0.20	0.37 ± 0.17	0.38 ± 0.26
C-Helix	699-713	4.58 ± 0.21	3.23 ± 0.25	1.76 ± 0.11	1.90 ± 0.08	0.64 ± 0.13	0.76 ± 0.09
CTL	714-724	1.72 ± 0.19	1.23 ± 0.24	2.06 ± 0.12	1.97 ± 0.08	1.69 ± 0.13	1.82 ± 0.09

Table S3. Reduced Spectral Density Statistics for Holo WT and Holo S672R HCN4 (563-724) Samples

		$J(0) \times 10^9$ (s/rad)		$J(\omega_N) \times 10^{10}$ (s/rad)		$J(\omega_N + \omega_H) \times 10^{11}$ (s/rad)	
Region	**Residues**	**WT**	**S672R**	**WT**	**S672R**	**WT**	**S672R**
Total	563-724	4.04 ± 0.20	4.13 ± 0.29	1.64 ± 0.12	1.70 ± 0.13	0.39 ± 0.17	0.48 ± 0.14
β2-β3	621-636	3.94 ± 0.23	3.86 ± 0.23	1.62 ± 0.13	1.68 ± 0.12	0.24 ± 0.19	0.31 ± 0.13
BBR	639-652	3.70 ± 0.17	3.86 ± 0.20	1.66 ± 0.12	1.64 ± 0.09	0.42 ± 0.16	0.38 ± 0.10
PBC	659-676	4.21 ± 0.22	4.53 ± 0.43	1.62 ± 0.13	1.63 ± 0.17	0.29 ± 0.20	0.41 ± 0.18
C-helix	699-713	4.38 ± 0.17	4.65 ± 0.28	1.68 ± 0.14	1.77 ± 0.17	0.27 ± 0.19	0.39 ± 0.15
CTL	714-724	2.92 ± 0.18	3.23 ± 0.32	1.84 ± 0.10	1.99 ± 0.15	1.02 ± 0.12	1.21 ± 0.14

Supplemental Figures and Figure Captions

	PBC	*	*	*	*							*	*					
HCN4	659	G	E	I	C	L	L	T	R	G	R	R	T	A	S	V	R	A	D
HCN1	535	G	E	I	C	L	L	T	K	G	R	R	T	A	S	V	R	A	D
HCN2	604	G	E	I	C	L	L	T	R	G	R	R	T	A	S	V	R	A	D
HCN3	488	G	E	I	C	L	L	T	R	G	R	R	T	A	S	V	R	A	D
EPAC1	269	G	Q	L	A	L	V	N	D	A	P	R	A	A	T	I	I	L	R
EPAC2	404	G	K	L	A	L	V	N	D	A	P	R	A	A	S	I	V	L	R
PKA RIα CBD-A	199	G	E	L	A	L	I	Y	G	T	P	R	A	A	T	V	K	A	K
PKA RIα CBD-B	323	G	E	I	A	L	L	M	N	R	P	R	A	A	T	V	V	A	R
PKG RIβ CBD-A	182	G	E	L	A	I	L	Y	N	C	T	R	T	A	T	V	K	T	L

Fig S1. Multiple sequence alignment of the extended phosphate binding cassettes (PBCs) of mammalian CBDs. Residues that are fully conserved within at least three HCN isoforms are highlighted in gray, while those with similar side chain properties are highlighted in blue and those that are conserved among non-HCN CBDs are shown in green. The S672R mutation site is outlined with a red rectangle and the residues that form hydrogen bonds with cAMP in HCN4 are marked by asterisks along the top.

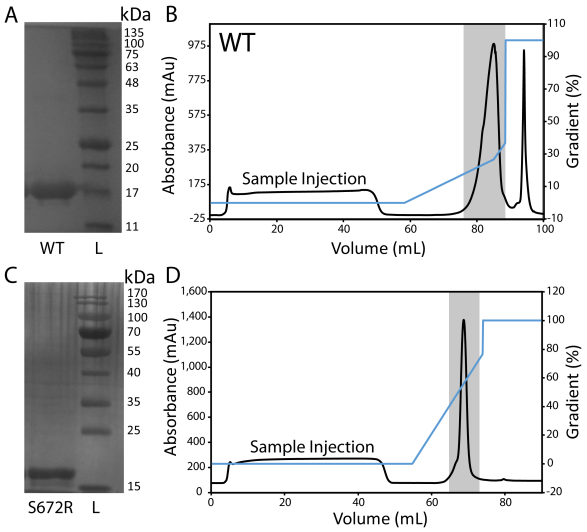

Fig S2. Purity of the WT and S672R HCN4 (563-724) constructs as assessed by SDS-PAGE and FPLC cation exchange chromatography. A) SDS-PAGE gel of WT HCN4 (563-724) with ladder (L). The expected molecular weight of this construct is ~18 kDa. **B)** FPLC chromatogram from cation exchange purification for WT HCN4 (563-724). The black line represents the absorbance at 254 nm, while the blue line depicts the gradient of Sp elution buffer (1M KCl). The gray box highlights the collected fractions of purified HCN that were used for NMR experiments. **C)** SDS-PAGE gel for a ~one year old S672R HCN4 (563-724) sample. **D)** Cation exchange chromatogram for S672R HCN4 (563-724).

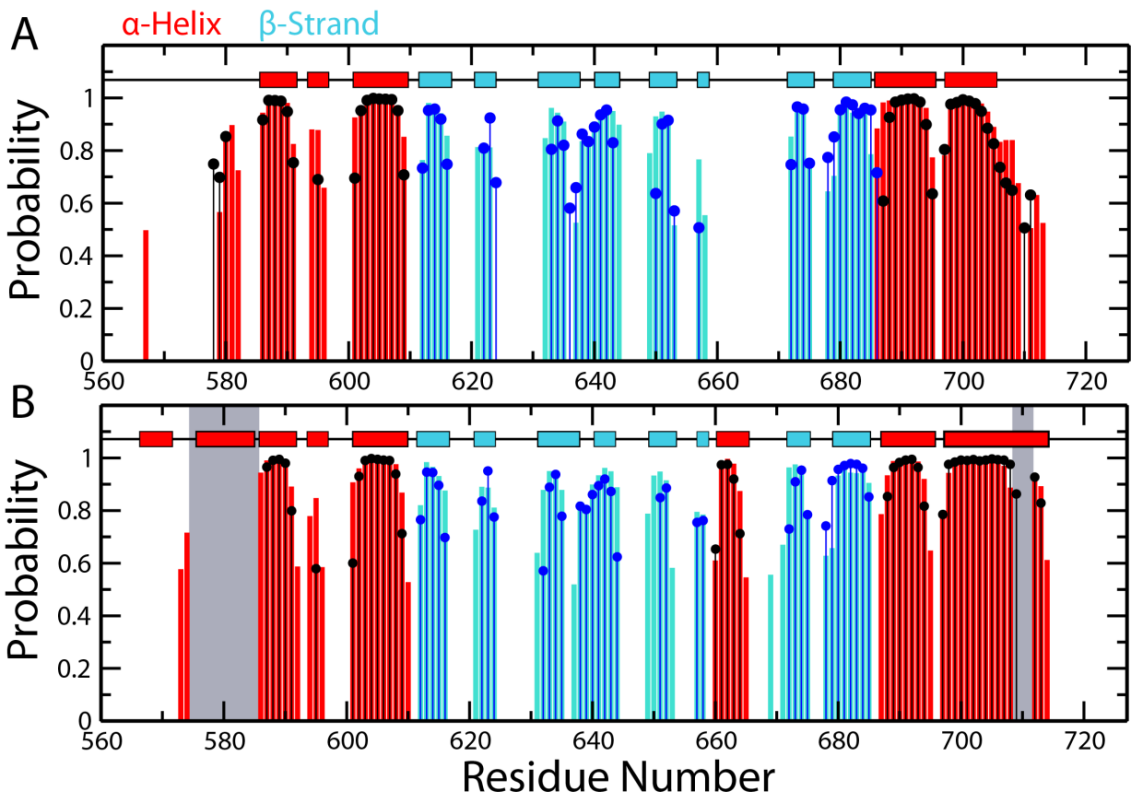

Fig S3. Secondary structure prediction for the wt and S672R CBDs of the HCN4 CBD using Talos+ [51] **with NH, Cα, Cβ and C' chemical shifts**. **A)** Secondary structure probabilities for the apo HCN4 CBD. The α-helices and β-strands are shown as red and cyan bars for the S672R mutant and as black and blue lines for the wt. The secondary structures from the apo solution structure of HCN4 (a.a. 579-707; PDB ID: 2MNG [9]) are depicted along the top using the same colour code as for the S672R secondary structure probabilities. **B)** Secondary structure prediction for the cAMP-bound state of the HCN4 CBD. Colour codes are the same as panel A. The secondary structure highlighted along the top of the plot was derived from the X-ray crystal structure of cAMP-bound HCN4 (a.a. 521-717; PDB ID: 3OTF [8]). Gray boxes highlight regions with incomplete chemical shift assignment.

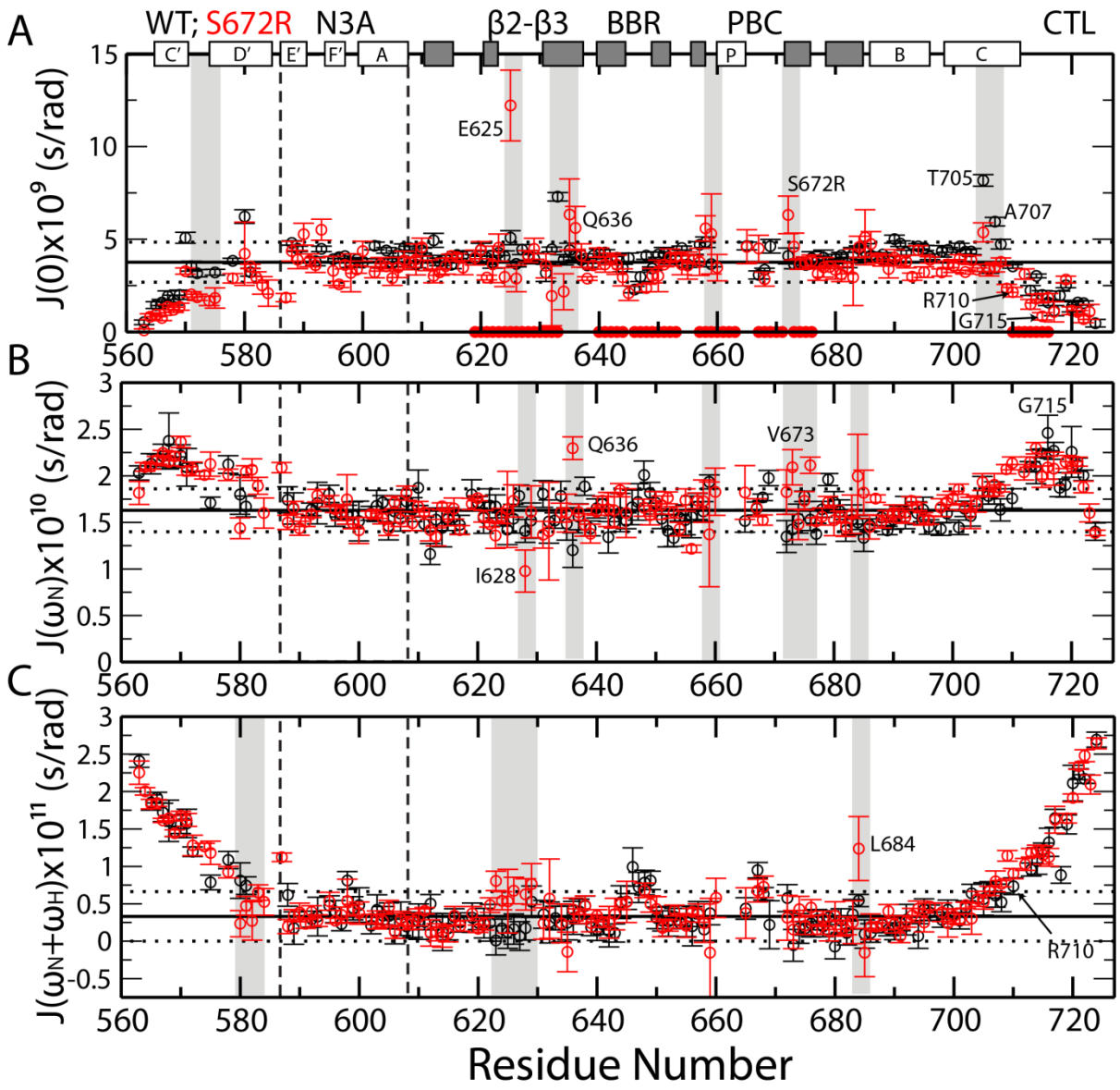

Fig S4. Reduced spectral densities for apo WT (black) and S672R (red) HCN4 (563-724). These spectral densities were computed from the R_1 and R_2 values, as well as heteronuclear $\{^1H\text{-}^{15}N\}$-NOEs (HN-NOEs) [9]. The secondary structure is depicted along the top of the J(0) plot as white (α-helices) and gray (β-strands) rectangles. The solid and dashed horizontal lines represent the average spectral density and the average value +/- five standard deviations, respectively, as explained in the main text. Selected residues subject to significant changes in dynamics are highlighted with gray boxes. The dashed vertical lines define the boundaries for the N3A motif.

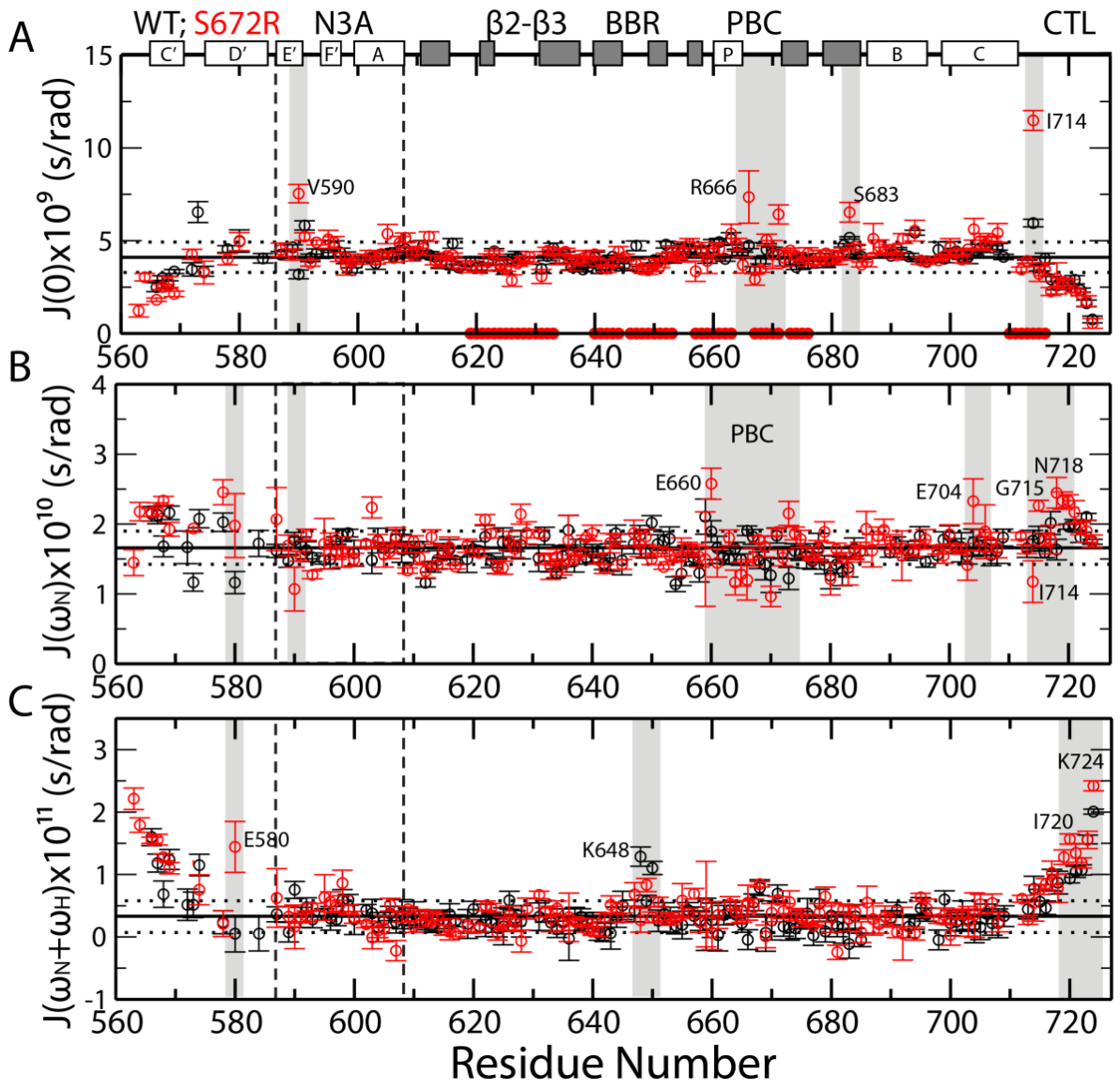

Fig S5. Reduced spectral densities for cAMP-bound WT (black) and S672R (red) HCN4 (563-724). Notations and color codes are as in Figure S4.

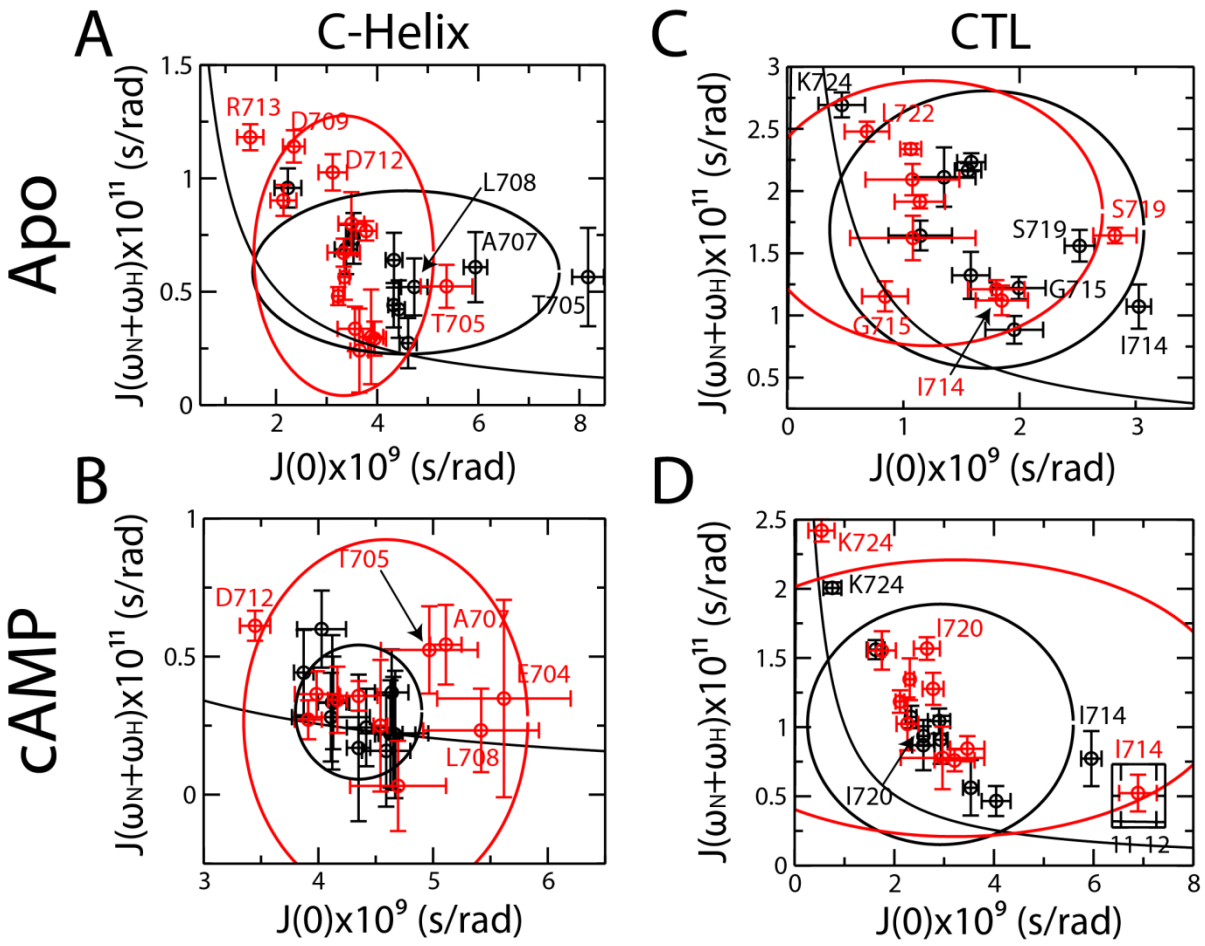

Fig S6. Two-dimensional reduced spectral densities plots for the C-Helix (a.a. 699 – 713) and CTL (a.a. 714 – 724). The layout is the same as in Fig 4, panels C-J.

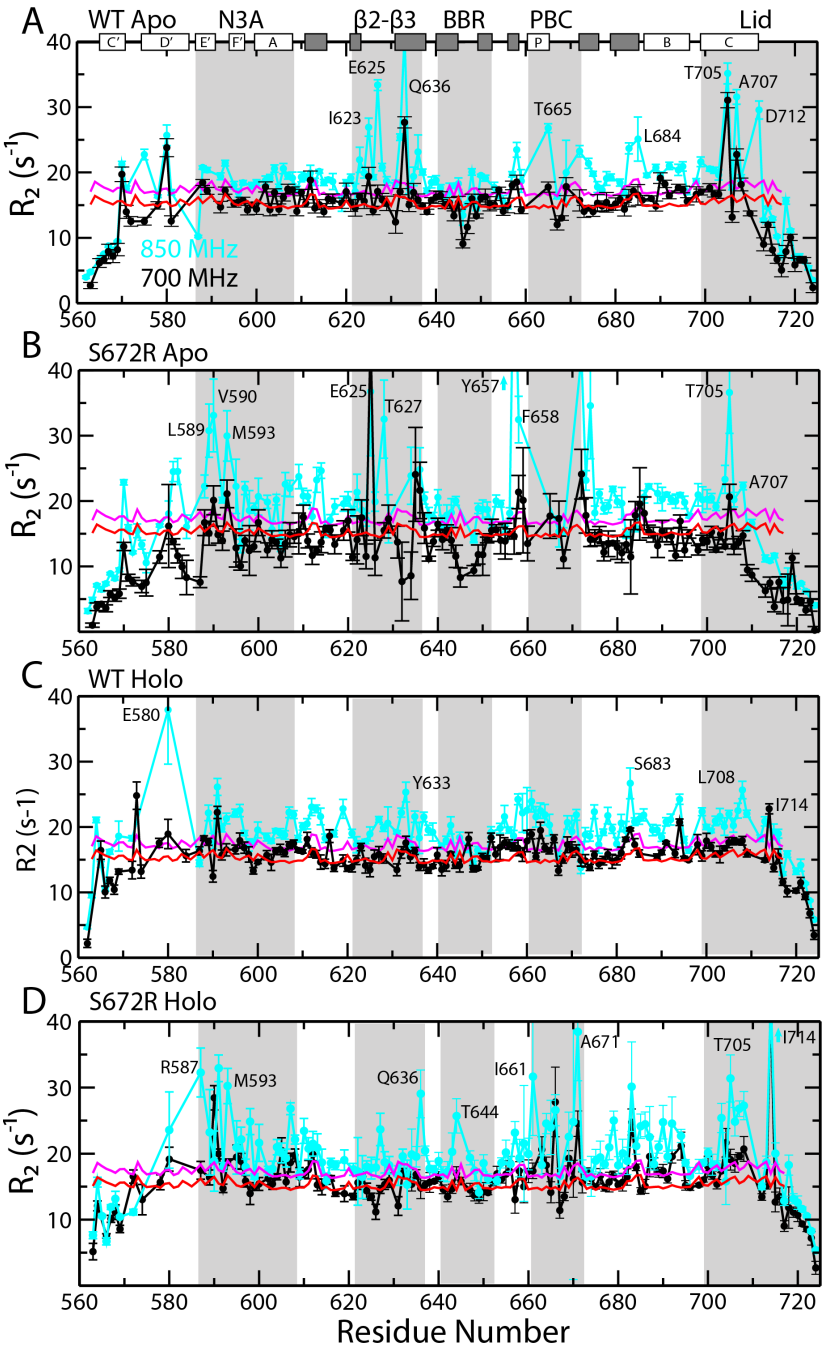

Fig S7. Comparison of R_2 relaxation rates at 850 MHz and 700 MHz for WT Apo (A), S672R Apo (B), WT cAMP-bound (C) and S672R cAMP-bound (D) HCN4. R_2 rates at 700 and 850 MHz are shown in black and cyan, respectively. The red and magenta lines depict the simulated R_2 rates, computed with HydroNMR[56], at 700 and 850 MHz, respectively.

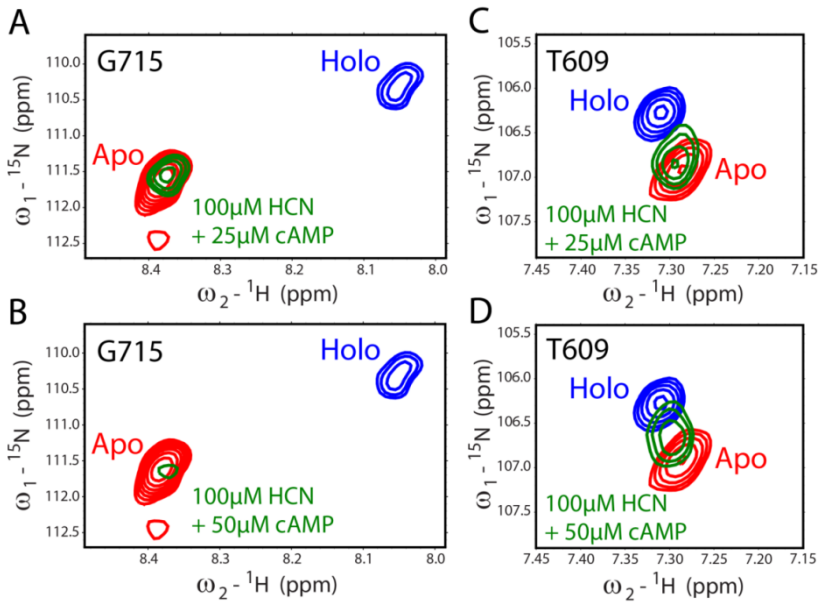

Fig S8. Evidence that residue G715 undergoes slow apo-holo exchange in the S672R HNC4 CBD. **A)** NH-HSQC spectra showing residue G715's apo (red), holo (blue) and partially bound (green) states. The lack of a partially bound peak at the position of the holo state raises the question of whether the G715 residue is in slow or fast exchange. **B)** The same spectra as panel A but after increasing the cAMP concentration from 25 to 50 μM. An increase in ligand concentration causes an increase in the exchange rate, which, if in the fast exchange regime, would cause sharper and more intense cross-peaks. In this spectra, however, there is a further broadening of the partially bound signal (green cross-peak), suggesting that in panel A, G715 was in the slow exchange and the increase in cAMP concentration drove the protein towards the intermediate exchange regime. The absence of the G715 holo peak for the partially bound sample in panel A likely reflects the fact that the holo state is only minimally populated and partially broadened. **C,D)** A similar analysis was performed for residue T609, which is already in the fast exchange regime at 25μM cAMP and therefore serves as a control. When the cAMP concentration was increased to 50μM (D), there was no major signal loss, unlike for G715.